BIOCHEMISTRY
including biophysical chemistry & molecular biology
Article

*Biochemistry* **XXXX,** *XXX,* 000–000 A
DOI: 10.1021/bi100390z

# Crystal Structure of Arginase from *Plasmodium falciparum* and Implications for L-Arginine Depletion in Malarial Infection[†,‡]

Daniel P. Dowling,[§] Monica Ilies,[§] Kellen L. Olszewski,[∥] Silvia Portugal,[⊥] Maria M. Mota,[⊥] Manuel Llinás,[∥] and David W. Christianson*[,§]

[§]*Roy and Diana Vagelos Laboratories, Department of Chemistry, University of Pennsylvania, Philadelphia, Pennsylvania 19104-6323,* [∥]*Department of Molecular Biology, Princeton University, Princeton, New Jersey 08544-1013, and* [⊥]*Unidade de Malária, Instituto de Medicina Molecular, Faculdade de Medicina Universidade de Lisboa, 1649-028 Lisboa, Portugal*

*Received March 13, 2010; Revised Manuscript Received May 25, 2010*

ABSTRACT: The 2.15 Å resolution crystal structure of arginase from *Plasmodium falciparum*, the parasite that causes cerebral malaria, is reported in complex with the boronic acid inhibitor 2(*S*)-amino-6-boronohexanoic acid (ABH) ($K_d$ = 11 $\mu$M). This is the first crystal structure of a parasitic arginase. Various protein constructs were explored to identify an optimally active enzyme form for inhibition and structural studies and to probe the structure and function of two polypeptide insertions unique to malarial arginase: a 74-residue low-complexity region contained in loop L2 and an 11-residue segment contained in loop L8. Structural studies indicate that the low-complexity region is largely disordered and is oriented away from the trimer interface; its deletion does not significantly compromise enzyme activity. The loop L8 insertion is located at the trimer interface and makes several intra- and intermolecular interactions important for enzyme function. In addition, we also demonstrate that *arg- Plasmodium berghei* sporozoites show significantly decreased liver infectivity in vivo. Therefore, inhibition of malarial arginase may serve as a possible candidate for antimalarial therapy against liver-stage infection, and ABH may serve as a lead for the development of inhibitors.

Malaria, an infectious disease caused by a parasitic protozoan, is a serious health threat in developing countries because of its facile transmission by the *Anopheles* mosquito (*1*, *2*). Malaria is currently considered to be eradicated in the United States; however, 10 species of *Anopheles* mosquitoes are indigenous to the United States, suggesting that malaria acquired in endemic countries can be reintroduced into the United States by human travel and propagated by mosquitoes. For example, there were 1505 cases of malaria diagnosed in the United States in 2007, including one transfusion-related case and one fatality (*3*). Worldwide statistics are significantly more severe, with 243 million cases of malaria being diagnosed and 863000 deaths resulting in 2008 (primarily children in sub-Saharan Africa) (*4*). Five species of malaria specifically infect humans: *Plasmodium falciparum*, *Plasmodium vivax*, *Plasmodium malariae*, *Plasmodium ovale*, and *Plasmodium knowlesi*; *P. falciparum* is the most lethal (*5*). Because the parasite is capable of developing resistance to drug therapy, combination drug therapies are generally required to circumvent this problem (*6*, *7*).

Malarial infection drastically alters host metabolism since the parasite co-opts essential nutrients for its own survival at the expense of a human host; moreover, the parasite introduces waste products and toxins into the circulatory system of the host (*8*). The pathogenic course of the disease is characterized by rapidly proliferating parasite cells, massive erythrocyte lysis, and ischemia (*9*). Clinical manifestations of malaria include hypoglycemia, lactic acidosis, hemolytic anemia, hemoglobinuria, and hypoargininemia (*9*).

Malaria patients often present with hypoargininemia (*10*, *11*), and metabolomic studies of *P. falciparum* during its 48 h intraerythrocytic life cycle reveal nearly complete depletion of L-arginine levels (*12*). Consistent with this observation, *P. falciparum* infection does not affect the influx kinetics of L-arginine in erythrocytes (*13*). Low levels of L-arginine correlate with decreased levels of immunity and nitric oxide (NO)[1] production (*14*). The depletion of L-arginine in culture is achieved by an arginase from the malarial parasite, which catalyzes the hydrolysis of the side chain guanidinium group to form L-ornithine and urea (*12*). Increased arginase activity characterizes the alternative immune response, which downregulates inflammation and tissue damage while upregulating angiogenesis and tissue repair mechanisms (*15*). Such conditions favor parasite growth through suppressed T cell and inflammatory responses to pathogens and increased concentrations of L-ornithine-derived polyamines, which facilitate cellular proliferation (*15*).

Increased exogenous arginase activity also characterizes infections by the parasitic protozoan *Leishmania major* and the

[†]This work was supported by National Institutes of Health (NIH) Grant GM49758 (D.W.C.), an NIH Director's New Innovator Award (1DP2OD001315-01 to M.L.), the Burroughs Wellcome Fund (M.L.), a National Science Foundation Graduate Research Fellowship (K.L.O.), the Howard Hughes Medical Institute (M.M.M.), and the Fundação para a Ciência e Tecnologia (FCT, Portugal) (S.P. and M.M.M.).

[‡]The atomic coordinates of the *P. falciparum* arginase−ABH complex have been deposited in the Protein Data Bank as entry 3MMR.

*To whom correspondence should be addressed. Telephone: (215) 898-5714. Fax: (215) 573-2201. E-mail: chris@sas.upenn.edu.

[1]Abbreviations: ABH, 2(*S*)-amino-6-boronohexanoic acid; BME, $\beta$-mercaptoethanol; hAI and hAII, human arginases I and II, respectively; dN-PFA, PFA beginning at residue K22 bearing an N-terminal His tag; L2S, PFA construct containing a 70-residue deletion in the L2 loop; LCR, low-complexity region; MPD, 2-methyl-2,4-pentanediol; NO, nitric oxide; PFA, *P. falciparum* arginase; PMSF, phenylmethanesulfonyl fluoride; rmsd, root-mean-square deviation; TAME, tosyl-arginine methyl ester; TCEP, tris(2-carboxyethyl)phosphine hydrochloride.

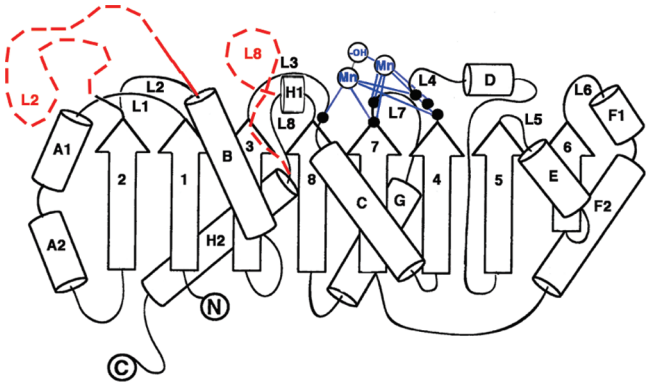


FIGURE 1: Topology diagram of human arginase I (hAI) and *P. falciparum* arginase (PFA). The positions of metal ligands are indicated by black spheres. Amino acid insertions within loops L2 and L8 of PFA relative to hAI are indicated by red dashed lines; the large ~70-residue insertion in the L2 loop is an asparagine-rich low-complexity region (LCR).

bacterium *Helicobacter pylori* (*16*−*18*). Consequently, the *arg*-variants of these organisms do not deplete host L-arginine levels and are accordingly more susceptible to the NO-dependent immune response. Decreased L-arginine levels have been observed in malaria patients, and supplemental L-arginine improves endothelial function in patients with moderate to severe malaria (*11*, *19*). Arginase activity is also implicated in slowing the recovery of malaria patients during treatment (*20*). Considering that current patient outcomes within the first 48 h of therapy do not change between quinine and artesunate treatment, it is proposed that treating endothelial dysfunction by targeting *P. falciparum* arginase with inhibitors within this time frame may represent a possible adjuvant therapy (*20*).

The *P. falciparum* arginase gene has been cloned and characterized (*21*, *22*). The amino acid sequence of arginase from *P. falciparum* is 28 and 27% identical with those of human arginases I (hAI) and II (hAII), respectively. Like the human arginases, *P. falciparum* arginase (PFA) is a binuclear manganese metalloenzyme that exists as a trimer with optimal activity at basic pH (*21*). Unlike the human arginases, PFA contains a large, 74-residue low-complexity region (LCR) inserted within loop L2 (Figure 1). Amino acid sequence alignments of arginases from *P. falciparum*, *P. vivax*, *Plasmodium yoelii*, *P. knowlesi*, and *Plasmodium berghei* reveal that this insert is as large as 100 residues in *P. vivax* and as small as 15 residues in *P. berghei* and shows no significant sequence conservation (*22*). Such LCRs are found in more than 90% of all proteins in the *P. falciparum* genome (*23*−*26*). A second ~11-residue insert is also located in loop L8 (Figure 1) (*22*). Despite these polypeptide insertions, PFA still exists as an active trimer (*21*). The question remains as to what effects, if any, these polypeptide insertions have on arginase structure and function. Kinetic measurements on a PFA construct bearing a C-terminal streptavidin affinity tag initially suggested that malarial arginase is less catalytically efficient than the mammalian arginases, with a $k_{cat}/K_M$ value of $7.4 \times 10^3$ $M^{-1}$ $s^{-1}$ (*21*) [compared with a $k_{cat}/K_M$ of $2.0 \times 10^5$ $M^{-1}$ $s^{-1}$ for rat arginase I (*27*) or $1.27 \times 10^5$ $M^{-1}$ $s^{-1}$ for hAI (*28*)].

Here, we report the preparation of a PFA construct bearing an N-terminal histidine tag instead of a C-terminal streptavidin affinity tag to facilitate purification. Kinetic studies with this new construct show that PFA actually exhibits catalytic efficiency comparable to that of hAI. The 2.15 Å resolution crystal structure of PFA in a complex with the boronic acid inhibitor 2(*S*)-amino-6-boronohexanoic acid (ABH) (*29*) reveals a binding mode comparable to that observed in the hAI−ABH complex (*30*) despite significantly weaker inhibitor binding affinity. Structural comparisons among mammalian, bacterial, and parasitic arginases reveal intriguing differences in the stabilization of oligomeric structure, and possible functions for the two polypeptide insertions in PFA are explored. Finally, the study of *arg*-*P. berghei* sporozoites confirms the importance of arginase activity in the mechanism of infection, suggesting that inhibition of malarial arginase may serve as a possible candidate for antimalarial therapy against liver-stage infection.

## MATERIALS AND METHODS

*P. falciparum Arginase Constructs*. The previously reported *P. falciparum* arginase construct (*21*, *22*) utilized the entire *P. falciparum* arginase gene with a C-terminal streptavidin affinity tag (PFA-Strep). Here, we report the preparation and analysis of three new arginase constructs: full-length PFA bearing a C-terminal histidine (His) tag (PFA-C6H), an N-terminal truncation beginning with K22 and bearing an N-terminal His tag (dN-PFA), and a similar N-terminal truncation with residues N84−D157 of loop L2 deleted (dN-PFA-L2S). Additionally, the H381A variant and the L8 chimera (in which loop L8 is replaced with the shorter hAI sequence) were generated from the dN-PFA plasmid. Restriction enzymes and ligase were purchased from New England Biosciences. Taq Hifi Polymerase was purchased from Invitrogen. All cell lines were purchased from Stratagene.

The PFA-C6H plasmid was constructed by first amplifying the *P. falciparum* arginase coding sequence from parasite genomic DNA (3D7 strain) with primers designed to incorporate a 5′ *Nhe*I site in place of the start codon and a 5′ *Xho*I site in place of the stop codon [primer 1, GCT AGC TTG GAT ACT ATA GAA AGT TAC ATC; primer 2, CTC GAG CAC TAT ATC GTA TCC TAA CAC (restriction sites underlined)]. This amplicon was cloned into the pET24a plasmid to give a recombinant gene with an N-terminal Met-Ala-Ser in place of the initial Met and a C-terminal Leu-Glu-6His tag.

To generate dN-PFA, the arginase gene was amplified from the C-terminal His-tagged construct PFA-C6H. NheI and HindIII restriction sites were incorporated to delete the first 21 amino acids [primer 1, GAG CGC TAG CAA AAA CGT TTC CAT TAT TGG TTC TCC; primer 2, CTC AAG CTT TTA CAC TAT ATC GTA TCC (restriction sites underlined)]. Deletion of the corresponding N-terminal segment of hAII facilitated its crystallization (*31*), so we reasoned that a comparable deletion would facilitate the crystallization of PFA. The digested PCR product was ligated into PET28a (Novagen), utilizing the N-terminal His tag and thrombin cleavage site, and transformed into XL-1 Blue cells for DNA isolation and sequencing. For the L2 loop deletion construct (dN-PFA-L2S), an AgeI restriction site was incorporated into the dN(1−21) construct L2 loop, resulting in the deletion of residues N84−D157 [primer 1, CGG ACC GGT AAT ATA AGG AAT ATA AA; primer 2, CGG ACC GGT TTT TTT TTC TTG TTT CAT (restriction sites underlined)]. The digested product was purified using a Qiagen extraction kit and transformed into XL-1 Blue cells for DNA isolation and sequencing. Sequencing was performed by the University of Pennsylvania DNA Sequencing Facility, and the identified positive clone was then transformed into *Escherichia coli* BL21-CodonPlus(DE3)-RIL cells for expression as previously described (*21*).

Table 1: Kinetic Parameters for *P. falciparum* Arginase (PFA) Constructs

| construct | pH | $K_M$ (mM) | $k_{cat}$ ($s^{-1}$) | $k_{cat}/K_M$ ($M^{-1}$ $s^{-1}$) | $K_i$(ABH) ($\mu$M) |
|---|---|---|---|---|---|
| dN-PFA[a] | 8.5 | 3.3 ± 0.6 | 440 ± 20 | (1.3 ± 0.2) × $10^5$ | 10 ± 1 |
| | 8.0 | 4 ± 1 | 320 ± 40 | (8 ± 2) × $10^4$ | 12 ± 2 |
| | 7.4 | 25 ± 2 | 77 ± 2 | (3.0 ± 0.3) × $10^3$ | 11 ± 2 |
| PFA-C6H | 8.0 | 12 ± 1 | 76 ± 7 | (2.9 ± 0.4) × $10^3$ | ND[b] |
| PFA-Strep[c] | 8.0 | 13 | 96 | 7.4 × $10^3$ | ND[b] |
| dN-PFA-L2S | 8.0 | 4.0 ± 0.3 | ND[b,d] | ND[b] | ND[b] |
| dN-PFA-H381A | 8.0 | 10 ± 1 | 28 ± 2 | (2.7 ± 0.3) × $10^3$ | 53 ± 2 |
| dN-PFA L8 chimera[e] | 8.0 | 20 ± 4 | ND[b,f] | ND[b] | ND[b] |
| human arginase I[g] | 9.0 | 1.5 | 190 | 1.27 × $10^5$ | 0.005[h] |

[a]dN-PFA signifies the N-terminally truncated form of PFA based on sequence alignment with hAII. The N-terminal His tag is not cleaved. [b]Not determined. [c]From ref *21*. [d]$V_{max}$ = 2.3 ± 0.1 $\mu$M/s. [e]dN-PFA L8 chimera shows substrate inhibition with a $K_i$ of 130 ± 50 mM. [f]$V_{max}$ = 2.6 ± 0.5 $\mu$M/s. [g]From ref *28*. [h]From ref *30*; dissociation constant ($K_d$) determined by isothermal titration calorimetry.

The H381A variant was generated using the QuikChange mutagenesis kit (Stratagene) with the dN-PFA template (primer 1, 5′-GTT GAT AAA AAA GTT gcT GGA GAT TCA TTG CC-3′; primer 2, 5′-GGC AAT GAA TCT CCA gcA ACT TTT TTA TCA AC-3′). The PCR product was transformed into XL1-Blue cells for DNA isolation and sequencing. The construct for the L8 chimera was generated utilizing TA overhangs generated by Platinum Taq (Invitrogen) polymerase. The dN-PFA plasmid without residues D374−T392 was elongated (primer 1, 5′-AAA ACA GGC AAG TTG TGT TTA GAA CTT ATC GCC-3′; primer 2, 5′-CCC AAG TGA TGG ATT ATA TTC TAC TAA ATC C-3′). The insert was purchased from IDT (primer 3, 5′-AG ACA CCA GAA GAA GTA ACT-3′; primer 4, 5′-GTT ACT TCT TCT GGT GTC TT-3′) and annealed separately before being ligated with the PCR product. The ligation product was transformed into XL-1 Blue cells for DNA isolation and sequencing, and the identified positive clone was then transformed into *E. coli* BL21-CodonPlus(DE3)-RIL cells for expression as previously described (*21*).

*Protein Expression and Purification*. Briefly, transformed or streaked cells were grown on Luria-Bertani (LB) agar supplemented with 50 $\mu$g/mL kanamycin. The LB medium supplemented with 50 $\mu$g/mL kanamycin was inoculated with a single colony and grown for 8 h at 37 °C and 250 rpm. This starter culture was then transferred to 250 mL of LB medium supplemented with 50 $\mu$g/mL kanamycin and 34 $\mu$g/mL chloramphenicol and grown for 12−16 h. The 250 mL cell growth was used to inoculate 5 L of either LB or minimal medium supplemented with 50 $\mu$g/mL kanamycin. Cells were induced with 1 mM IPTG in the presence of 50 $\mu$g/mL kanamycin, 10 $\mu$g/mL phenylmethanesulfonyl fluoride (PMSF), and 1 $\mu$g/mL tosyl-arginine methyl ester (TAME) at 37 °C.

Cells were harvested by centrifugation at 6000*g* and resuspended in 50 mM Tris (pH 8.0), 500 mM NaCl, and 3 mM $\beta$-mercaptoethanol (BME) in the presence of protease inhibitors (10 $\mu$g/mL PMSF and 1 $\mu$g/mL TAME). Cells were lysed by sonication and centrifuged at 30000*g* for 1 h. The supernatant was loaded onto Ni-nitrilotriacetic acid resin and eluted with increasing imidazole concentrations (10, 50, and 200 mM). Pulled protein fractions were dialyzed into 50 mM Tris (pH 8.0), 200 mM NaCl, 1 mM $MnCl_2$, and 1 mM tris(2-carboxyethyl)-phosphine (TCEP) and subsequently concentrated. Protein was loaded onto a Superdex 26/60 size exclusion column preequilibrated with dialysis buffer. The trimer protein peak was collected, concentrated, and stored in aliquots at 4 °C.

*Kinetic Assays*. dN-PFA, dN-PFA-L2S, dN-PFA L8 chimera, dN-PFA-H381A, and PFA-C6H were assayed for catalytic activity using a colorimetric method (*32*) with slight modifications. The reaction of urea with α-isonitroso propiophenone was assessed at a wavelength of 550 nm using the Envision plate reader (courtesy of the S. Diamond laboratory, Institute of Medicine and Engineering, University of Pennsylvania). Product formation was assessed by means of urea standard curves. No background signal from substrate reacting with α-isonitroso propiophenone was observed when up to 400 mM L-arginine was used. At L-arginine concentrations of > 100 mM, a decrease was observed for the dye developing reaction; therefore, standard curves containing stoichiometric ratios of urea and L-arginine were used for reactions with > 100 mM L-arginine. The arginase reaction was performed in 50 mM Tris (pH 8.0), 0.5 mM TCEP, 1 mM $MnCl_2$, 0.05−1 $\mu$M protein, and 1−200 mM L-arginine for 5−10 min at 37 °C. The assay mixture and protein were preincubated at 37 °C for > 1 min before the reaction was initiated. The assay mixture (20 $\mu$L) was stopped with a sulfuric-phosphoric acid/α-isonitroso propiophenone mixture (140 $\mu$L). Reaction points were developed in a thermocycler (90 °C for 1 h), followed by incubation at room temperature (21 °C for 15 min). The dN-PFA expressed in minimal medium exhibited increased activity and was used for $k_{cat}$ calculations as measured by linear rates at 200 mM L-arginine with 50 nM protein. Kinetic parameters were determined with Graphpad Prism (2008). Inhibition studies were performed with 25 mM L-arginine at 37 °C for 10 min to obtain significant absorbance signals to plot $IC_{50}$ data. The $K_i$ value for ABH was calculated using the Cheng−Prusoff equation (*33*). Results are listed in Table 1.

*Isothermal Titration Calorimetry of Formation of the dN-PFA−ABH Complex*. Experiments were conducted on an ITC200 isothermal calorimeter from MicroCal, Inc., in the laboratory of W. DeGrado at the University of Pennsylvania. Enzyme (50 $\mu$M) was dialyzed against 50 mM Tris (pH 8.0), 200 mM NaCl, 1 mM $MnCl_2$, and 1 mM TCEP; 0.65 mM ABH was dissolved in dialysis buffer. The sample cell (0.3 mL) was overfilled, and the reference cell was filled with distilled water. The inhibitor ABH was titrated into the sample cell with 20 sequential aliquots (2 $\mu$L each; an initial 0.2 $\mu$L injection was made, but not used in data analysis). A control experiment titrating the inhibitor into buffer was subtracted out, and data analysis was performed using ORIGIN version 7.0.

*Crystallography*. The inhibitor ABH was synthesized as previously described (*29*). The construct dN-PFA was used successfully in crystallization experiments. Briefly, a 2 $\mu$L sitting drop of 5−10 mg/mL dN-PFA in 50 mM Tris (pH 8.0), 200 mM NaCl, 1 mM $MnCl_2$, 1 mM TCEP, and 5 mM ABH was mixed with a drop of 1.4 M sodium/potassium phosphate (pH 8.2) and

Table 2: Data Collection and Refinement Statistics

| | |
|---|---|
| **Data Statistics** | |
| resolution limits (Å) | 37−2.15 |
| space group | *R*32 (hexagonal) |
| *a*, *b*, *c* (Å) | 112.5, 112.5, 228.7 |
| total no. of reflections | 59546 |
| no. of unique reflections | 31095 |
| completeness (%) (overall/outer shell) | 100/100 |
| redundancy (overall/outer shell) | 8.4/8.3 |
| $R_{merge}$[a] (overall/outer shell) | 0.104/0.420 |
| $I/\sigma(I)$ (overall/outer shell) | 19.4/5.4 |
| **Refinement** | |
| $R/R_{free}$[b] | 0.155/0.186 |
| no. of atoms | |
| protein atoms[c,d] | 2440 |
| water molecules[c] | 298 |
| ligand atoms[c] | 13 |
| metal ions[c] | 2 |
| BME atoms | 4 |
| average *B* factor (Å$^2$) | |
| main chain | 30 |
| side chain | 34 |
| water molecules | 43 |
| $Mn^{2+}$ ions | 21 |
| inhibitor | 33 |
| BME | 38 |
| Ramachandran plot (%) | |
| most favorable | 90.0 |
| additional allowed | 10.0 |
| generously allowed | 0.0 |
| disallowed | 0.0 |
| rmsd | |
| bond lengths (Å) | 0.007 |
| bond angles (deg) | 1.1 |
| dihedral angles (deg) | 17.1 |

[a] $R_{merge} = \sum|I - \langle I\rangle|/\sum I$, where $I$ is the observed intensity and $\langle I\rangle$ is the average intensity calculated for replicate data. [b] Crystallographic *R* factor ($R = \sum||F_o| - |F_c||/\sum|F_o|$) for reflections contained in the working set. Free *R* factor ($R_{free} = \sum||F_o| - |F_c||/\sum|F_o|$) for reflections contained in the test set excluded from refinement. $|F_o|$ and $|F_c|$ are the observed and calculated structure factor amplitudes, respectively. [c] Per asymmetric unit. [d] Residue C154 refined with an occupancy of 0.5.

equilibrated against a 500 $\mu$L reservoir of 40−50% 2-methyl-2, 4-pentanediol (MPD) at room temperature. Small crystals appeared overnight and grew to typical dimensions of 50 $\mu$m × 50 $\mu$m × 50 $\mu$m. Crystals were harvested and cryoprotected in 30% Jeffamine ED-2001 and 0.1 M HEPES (pH 7.0) and then flash-cooled in liquid nitrogen. Diffraction data were measured on beamline 24-ID-E at the Advanced Photon Source (APS, Argonne, IL). Crystal parameters and data collection statistics are listed in Table 2.

Data were indexed and merged using HKL2000 (*34*). Molecular replacement calculations were performed with PHASER (*35*) using the atomic coordinates of hAII less inhibitor and solvent atoms [Protein Data Bank (PDB) entry 1PQ3] (*31*) as a search probe for rotation and translation function calculations. Iterative cycles of refinement and model building were performed using PHENIX (*36*) and COOT (*37*), respectively, to improve each structure as guided by $R_{free}$. The N-terminal His tag is completely disordered, and electron density is observable beginning at residue K22 of the dN-PFA protein sequence. Residues G72−N153 of the L2 loop insert are disordered and excluded from the final model. Two cis-peptide linkages are found in the refined structure: residues G190 and G191 immediately after $\beta$3 and residues G382 and D383 within the loop L8 insert. All refinement statistics are listed in Table 2. Buried surface area calculations were performed using the PISA server (http://www.ebi.ac.uk/msd-srv/prot_int/pistart.html) (*38*).

*Mice and Plasmodium Liver Infection*. C57BL/6 mice were housed in the Instituto de Medicina Molecular (IMM) facilities, and experiments were performed under IMM Animal Care Committee approval following National and EU guidelines. The *arg*- (*12*) and wild-type *P. berghei* sporozoites were obtained by dissection of *Anopheles stephensi*-infected mosquitoes bred at the IMM insectarium. Mice were infected by intravenous inoculation of $3 \times 10^4$ sporozoites, and the parasite liver load was quantified 40 h postinfection by quantitative RT-PCR, as previously described (*39*). The relative amount of *P. berghei* ANKA 18S rRNA was calculated against the hypoxanthine guanine phosphoribosyltransferase (hprt) housekeeping gene. The PbA 18S rRNA and hprt specific primer sequences were 5′-CGG CTT AAT TTG ACT CAA CAC G-3′ and 5′-TTA GCA TGC CAG AGT CTC GTT C-3′ for PbA 18S rRNA and 5′-TGC TCGAGA TGT GAT GAA GG-3′ and 5′-TCC CCT GTT GAC TGG TCA TT-3′ for mouse hprt, respectively. External standardization was performed using plasmids encoding the full-length *P. berghei* 18S rRNA and hprt cDNA cloned into TOPO TA (Invitrogen).

## RESULTS AND DISCUSSION

*Catalytic Activity of PFA Constructs*. The catalytic efficiency ($k_{cat}/K_M$) of dN-PFA increases with an increase in pH, and kinetic parameters are comparable to those measured for human arginase I (Table 1). Importantly, the dN-PFA construct is the most catalytically active form of PFA reported to date. While the $K_M$ values measured for the PFA constructs reported in Table 1 are in the same range as the $K_M$ values measured for mammalian arginases [$K_M$ = 1.4 mM for rat arginase I at pH 9.0 (*40*); $K_M$ = 1.5 mM for hAI at pH 9.0 (*41*), and $K_M$ = 0.55 mM for hAII at pH 9 (*42*)], the $K_M$ value of 12 mM measured for the PFA-C6H construct at pH 8.0 and the $K_M$ value of 13 mM measured for the C-terminal streptavidin affinity tag construct reported by Müller and colleagues at pH 8.0 (PFA-Strep) (*21*) are notably higher. Therefore, it appears that a C-terminal affinity tag on PFA is detrimental for substrate binding and catalytic activity.

The tightest binding inhibitor of rat and human arginases known to date is the boronic acid analogue of L-arginine, ABH (*29*), which inhibits hAI with a $K_d$ of 5 nM (*30*). Indeed, ABH is an orally bioavailable drug lead that shows promising in vivo activity for the treatment of cardiovascular diseases such as erectile dysfunction and atherosclerosis in animal models (*31*, *43*). However, the inhibition of dN-PFA by ABH at physiological pH is significantly weaker, with a $K_i$ of 11 ± 2 $\mu$M assuming competitive inhibition (Table 1). This affinity was confirmed by isothermal titration calorimetry (pH 8.0) with a $K_d$ of 11 ± 2 $\mu$M (Figure 2). The origin of weaker binding to dN-PFA is not evident in the crystal structure of the enzyme−inhibitor complex, since ABH appears to make identical interactions in the active sites of hAI and dN-PFA (vide infra).

To assess the functions of the two amino acid sequence inserts in PFA, two deletion constructs were generated. Approximately 70 residues (N84−D157) of the 74-residue LCR were deleted from the L2 loop to generate the dN-PFA-L2S construct. A survey of arginase crystal structures in the Protein Data Bank suggested that this deletion construct would be able to fold properly. Similarly, residues D374−T392 of loop L8 were replaced with

the corresponding sequence from human arginase I, yielding the dN-PFA-L8 chimera. While these constructs do not express well, soluble protein expression is confirmed by Western blotting analysis using an anti-His antibody (data not shown). Because of the significant decrease in protein purity and the level of expression, accurate protein concentrations were difficult to estimate. However, a $K_M$ value of 4.0 ± 0.3 mM was determined for the L2S construct with a $V_{max}$ of 2.3 ± 0.1 $\mu$M $s^{-1}$, and a $K_M$ value of 20 ± 4 mM was determined for the L8 chimera with a $V_{max}$ of 2.6 ± 0.5 $\mu$M $s^{-1}$. The $K_M$ value for the L2S construct is in accord with that measured for the dN-PFA construct, indicating that the LCR does not significantly impact substrate affinity. The L8 chimera shows moderately decreased substrate affinity; moreover, this construct shows substrate inhibition with a $K_i$ of 130 ± 50 mM (data not shown).

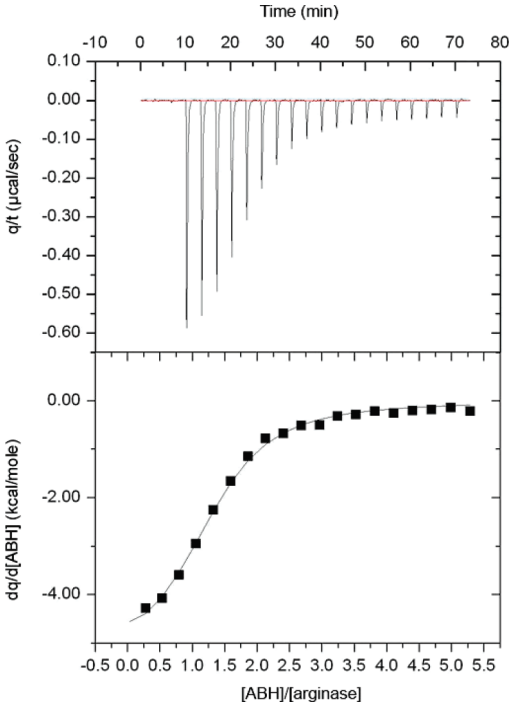


FIGURE 2: Isothermal titration calorimetry of the PFA−ABH complex in 50 mM Tris (pH 8.0), 200 mM NaCl, 1 mM TCEP, and 1 mM $MnCl_2$ at 25 °C. Shown are the raw data obtained by titration of 50 $\mu$M arginase with 20 × 2 $\mu$L injections of 650 $\mu$M ABH. The area under each peak is integrated and plotted vs [ABH]/[arginase]. The solid line represents the best fit of the experimental data using nonlinear least-squares fitting, indicating a stoichiometry $n$ of 1.27 ± 0.03, an association constant ($K_a$) of (8.8 ± 0.9) × $10^4$ $M^{-1}$ (and thus dissociation constant $K_d$ = 11 ± 2 $\mu$M), and a $\Delta H$ of −5.4 ± 0.2 kcal/mol.

Parasitic LCR inserts are expected to exist primarily as unstructured domains made up of hydrophilic and flexible amino acids such as Asn, Lys, Glu, and Asp (*26*), and this is the case for the 74-residue LCR in loop L2 of PFA. In PFA, the LCR insert does not affect substrate binding, and the protein readily crystallizes despite its presence (vide infra). While the possible functions of LCR inserts are not fully understood, they are thought to be external, nonglobular domains that do not necessarily affect protein function. However, examples are known in which LCR inserts affect enzyme activity and quaternary structure, including dihydrofolate reductase-thymidylate synthase, subtilisin-like protease-1, and *S*-adenosylmethionine decarboxylase/ornithine decarboxylase of *P. falciparum* (*44*−*46*).

*Crystal Structure*. Since the dN-PFA construct was utilized for the X-ray crystal structure determination, the acronym "PFA" refers specifically to this construct in the remainder of this paper. PFA crystallizes as a loosely associated dimer of trimers related by a crystallographic 2-fold axis. The observed quaternary structure is identical to that of the hexameric arginases from *Thermus thermophilus* and *Bacillus caldovelox* (*47*, *48*), except that there is less than 5% buried surface area between the symmetry-related trimers of PFA. Dynamic light scattering experiments indicate that PFA is a trimer in solution (data not shown).

The PFA−ABH and hAI−ABH monomers superimpose with a rmsd of 0.93 Å for 245 Cα residues. Significant structural differences are observed near the two sequence insertions in PFA (Figure 3a). While the 11-residue insert in loop L8 is well-ordered, the 74-residue LCR insert in loop L2 is largely disordered: only flanking residues D70, N71, and C154−N158 are modeled into visible electron density, and C154 is refined with half-occupancy. The LCR is distant from the active site and is oriented away from the trimer interface (Figure 3b). Thus, the LCR does not significantly impact enzyme structure or function.

The structure of the binuclear manganese cluster in the PFA−ABH complex is very similar to that observed in the rat and human arginase I complexes (*30*, *49*). Both metal ions exhibit distorted octahedral coordination geometry (Figure 4a). The

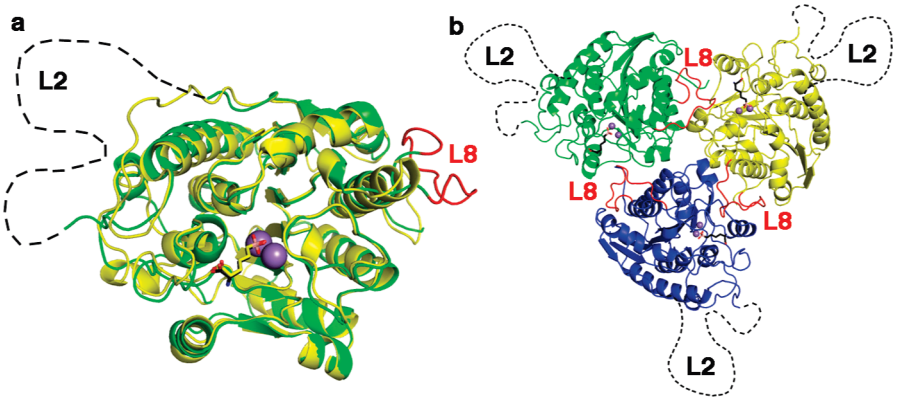


FIGURE 3: (a) Superposition of the hAI monomer [yellow, PDB entry 2AEB (*30*)] with the PFA monomer (green), both in complex with the inhibitor 2(*S*)-amino-6-boronohexanoic acid (ABH). $Mn^{2+}$ ions are shown as purple spheres, and the inhibitor ABH is colored as follows: C, yellow (hAI) or black (PFA); O, red; N, blue; B, orange. Structural differences are observed for amino acid inserts in PFA: loop L2 (disordered LCR, black dashed line) and loop L8 (red). (b) Trimeric PFA−ABH complex. Individual monomers are colored yellow, blue, and green; loops L2 and L8 are indicated as in panel a.

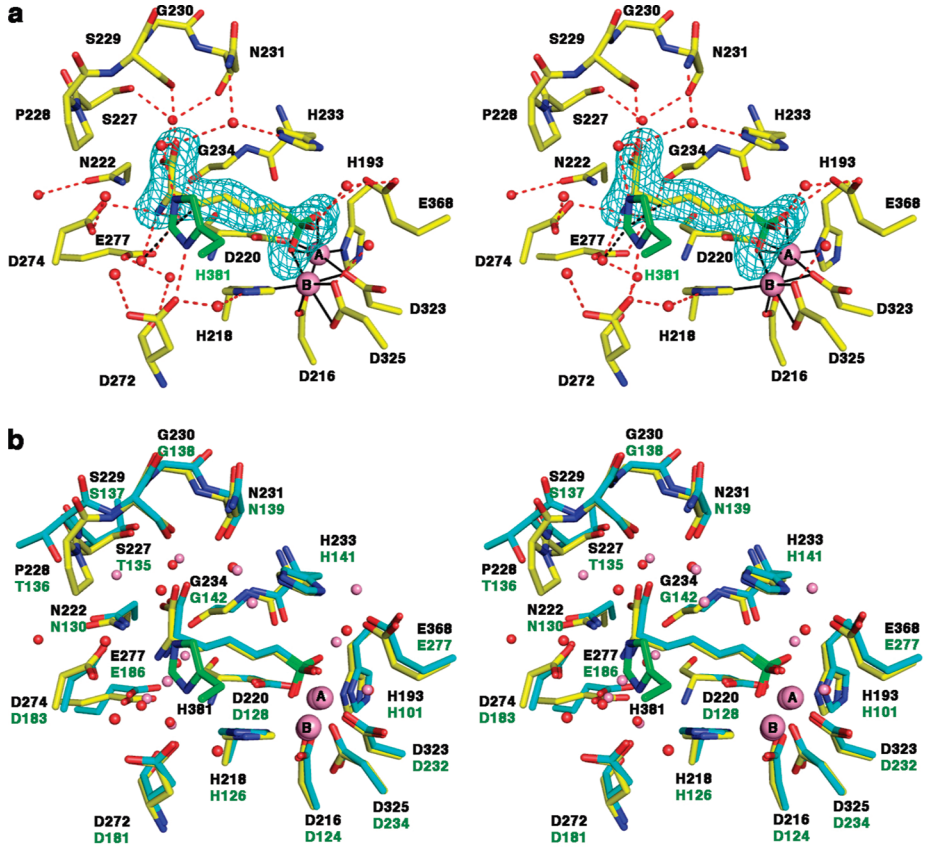


FIGURE 4: (a) Simulated annealing omit map of 2(*S*)-amino-6-boronohexanoic acid (ABH) contoured at 5$\sigma$. The binding mode of ABH is similar to that observed for binding to mammalian arginases (*30*, *59*). Intriguingly, $H381_B$ from an adjacent monomer (green) extends from the L8 loop insertion into the active site of monomer A. Metal coordination interactions are indicated by solid black lines; selected hydrogen bond and van der Waals interactions are indicated by dashed red and black lines, respectively. (b) Superposition of the PFA−ABH complex (colored as in panel a) with the hAI−ABH complex (cyan). PFA and hAI residue labels are black and green, respectively.

electron density for the inhibitor ABH indicates that the boronic acid moiety undergoes nucleophilic attack by the metal bridging hydroxide ion to yield a tetrahedral boronate anion. This binding mode mimics the tetrahedral intermediate and its flanking transition states in the hydrolysis of L-arginine (*50*).

The molecular recognition of the α-amino and α-carboxylate groups of ABH is mediated by several direct and water-mediated interactions with active site residues, most of which are also observed in the hAI−ABH complex (*30*) (Figure 4b). Water-mediated hydrogen bonds are particularly notable. Two water molecules interact with the α-amino group of ABH. One water molecule is within hydrogen bonding distance of E277 and the backbone C=O group of G234, and the other is within hydrogen bonding distance of the carboxylate side chains of D274 and D272 and the backbone C=O group of D272. This water molecule also makes a van der Waals contact with H381 (vide infra). Three water molecules are observed within hydrogen bonding distance of the α-carboxylate moiety of ABH and mediate interactions with S227, N231, H233, and H381 from an adjacent monomer.

Several hydrogen-bonded salt links in the bacterial and mammalian arginases are known to be important for stabilization of the trimeric quaternary structure (*27*, *41*, *51*, *52*), and some of these salt links are conserved in PFA. Specifically, at the center of the trimer interface, the hAI salt link network involving $D204_A$, $E256_A$, and $R255_B$ is conserved as $E295_A$, $E347_A$, and $R346_B$, respectively, in PFA (subscripts A and B indicate adjacent monomers) (Figure 5). The aspartate → glutamate substitution results in a conformational change that nonetheless maintains the hydrogen bond interaction with the central arginine residue. However, in hAI, $D204_A$ makes a syn-oriented hydrogen bond with $R255_B$, whereas in PFA, E295 makes an anti-oriented hydrogen bond with $R346_B$.

A second salt link network observed in mammalian arginases and the arginase from *T. thermophilus* is not conserved within PFA. This network consists of $D204_A$, $E262_B$, and $R308_B$ in hAI and is linked to the conserved salt link network described above through residue $D204_A$, which accepts hydrogen bonds from both $R255_B$ and $R308_B$ of an adjacent monomer (Figure 5). Interestingly, arginase from *B. caldovelox* does not contain the corresponding R308 residue, but a free L-arginine molecule is reported to bind and make interactions similar to those of R308 in the mammalian arginases (*47*).

The 11-residue insertion in loop L8 influences the structure and function of PFA. As previously noted in the structure determination of rat arginase I (*53*), the C-terminal polypeptide mediates more than 50% of the intermonomer contact surface area. The enlarged L8 loop of PFA precedes helix H2 and the C-terminal polypeptide and augments intermonomer contacts (Figures 3b and 6). Interestingly, $K340_A$ from loop L7 protrudes into a pocket in the adjacent monomer defined by residues from helices G and H2 and loop L8 ($Y345_B$, $D377_B$, $K378_B$, $D383_B$, $K393_B$, $K396_B$, and $E400_B$). Of these residues, only Y345 is conserved as Y254 in hAI, so it is clear that the complementary surface area at the subunit interface has evolved to accommodate the loop L8 insertion. Parenthetically, we note that electron density for the side chain of K378 was not as well-defined as for

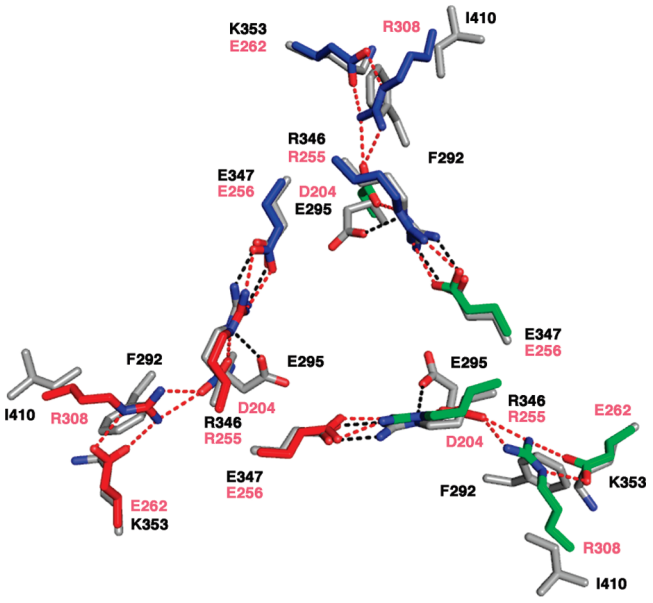


FIGURE 5: Arginase trimer containing several salt links at the trimer interface. The hAI subunit carbon atoms are colored red, blue, and green; oxygen and nitrogen atoms are colored red and blue, respectively. The PFA trimer subunits are colored similarly, except that carbon atoms are colored gray. The $R204_A$-$E256_B$-$D204_B$ salt links in hAI are conserved in PFA as $R346_A$-$E347_B$-$E295_B$ salt links. The second salt link cluster in hAI ($R308_A$-$E262_A$-$D204_B$) is replaced in PFA by $I410_A$, $K353_A$, $E295_B$, and $F292_B$.

other residues in this pocket. However, the main chain atoms of K378 were built into well-defined electron density, and the side chain was modeled with a conformation such that the Nζ atom was located near that of K340.

Another intermonomer interaction is observed for loop L8 of PFA, in that $H381_A$ is within hydrogen bonding distance of residue $D272_B$ in the active site; $H381_A$ also makes a solvent-mediated interaction with the carboxylate group of $ABH_B$ (Figures 3 and 4). Notably, $H381_A$ is 3.4 Å from the Cβ atom of the inhibitor molecule $ABH_B$, interacting through van der Waals interactions. A water molecule interacts with the α-amino group of $ABH_B$, $D272_B$, and $D274_B$ and is also located within hydrogen bonding distance of $H381_A$. Intermonomer interactions with the bound inhibitor are unique to the active site of PFA. Since H381 can make an intermonomer van der Waals contact with a bound inhibitor, it can also make a similar interaction with a bound substrate molecule. We probed the influence of H381 on enzyme activity by preparing the H381A variant, which exhibits modestly diminished kinetic parameters in comparison with those of dN-PFA; the binding affinity of ABH is also modestly compromised (Table 1). These results suggest that H381 contributes to substrate binding and catalysis.

Parenthetically, we note that a new intramonomer hydrogen bond network is observed in PFA involving $R404_A$, $E401_A$, and $Q349_A$ (Figure 6). Although these residues are located near the trimer interface, none make intermonomer interactions. However, the R404A mutation results in a partially active monomer (*22*), suggesting that the R404-E401-Q349 hydrogen bond network helps maintain the structure of the monomer near the subunit interface to facilitate trimer assembly.

*Altered Infectivity of arg- Parasites.* Previous work has suggested a possible connection between the plasmodial arginase and immune evasion by the parasite (*12*). However, disruption of the parasitic arginase in the rodent malaria model *P. berghei* does not compromise the in vivo viability in arginase knockout parasites; i.e., proliferation in blood-stage infection is not affected (*12*). This previous study used inoculations containing $10^6$ parasitized red blood cells to infect BALB/c mice. Here, we have compared the infectivity of *arg-* and wild-type *P. berghei* by inoculation of mice using sporozoites dissected from mosquito salivary glands. As opposed to direct infection with blood-stage parasites, sporozoites must first infect liver cells to produce merozoites that invade red blood cells and produce the manifestations of clinical malaria. Using qRT-PCR of *P. berghei* 18S rRNA to measure the degree of infectivity, we find a significant reduction ($p < 0.01$) in infectivity in the *arg-* strain 40 h postinfection (Figure 7), suggesting that liver-stage infection is compromised by parasite arginase deficiency. Wild-type *Plasmodium* sporozoites and developing liver forms express arginase (*arg*), which functionally degrades L-arginine. We hypothesize that during infection with wild-type parasites, L-arginine levels are lowered and as such the production of nitric oxide (NO) is likely reduced. This may allow the parasite to evade an NO-dependent immune response in the host. Indeed, the apparent reduction in

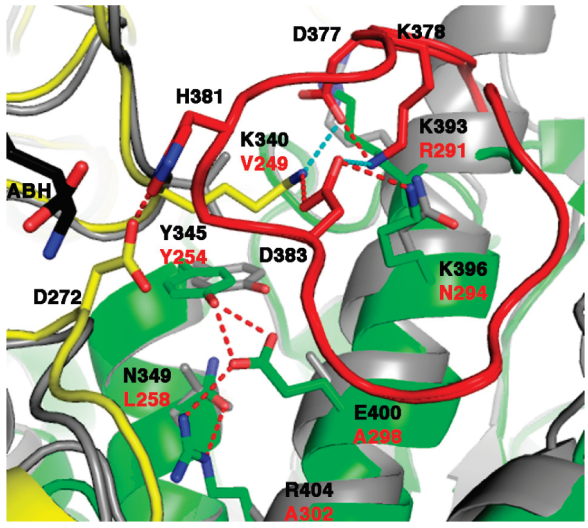


FIGURE 6: Unique inter- and intramonomer interactions involving loop L8 and helices G and H2 of PFA. PFA monomers are colored green and yellow, and the L8 loop is colored red. The superimposed hAI structure is colored gray. Red dashed lines represent hydrogen bonds and cyan dashed lines salt link interactions (~3.5−4 Å). Oxygen and nitrogen atoms are colored red and blue, respectively. Labels are black for PFA and red for hAI.

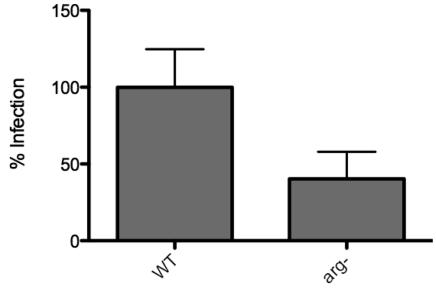


FIGURE 7: *P. berghei* sporozoite infection shows a dependency on plasmodial arginase expression. Sporozoites from wild-type (WT) and *arg-* (*12*) *P. berghei* strains were dissected from mosquito salivary glands and used to infect C57BL/6 mice. Data for WT and *arg-P. berghei* sporozoites show decreased infectivity in the *arg-* knockout ($p = 0.004$; $t = 40$ h). Error bars represent the standard deviation ($n = 7$).

liver-stage infection observed in *arg- P. berghei* parasites is consistent with this hypothesis, although an increase in the production of L-ornithine by the parasitic arginase may also be important for parasite survival. The decreased liver-stage infectivity of *arg-* parasites clearly warrants further investigation. Arginase inhibitors, perhaps in synergistic combination with inhibitors of parasite polyamine biosynthesis (*54*), may prove to be effective against liver-stage infection and may possibly serve as prophylactic agents in addition to their potential use as adjuvant therapies.

## CONCLUDING REMARKS

It is well documented that arginase activity can regulate NO biosynthesis and thereby facilitate immune evasion (*18*, *55*, *56*). The arginase can be that of the host, e.g., in certain cancer tumor cells (*57*) or circulating myeloid-derived suppressor cells in cancer patients (*56*), or it can be that of the invading pathogen, e.g., *H. pylori* arginase (*58*). In this work, disruption of *P. falciparum* arginase compromises the in vivo viability in arginase knockout sporozoites, possibly by weakening the ability of the parasite to modify the surrounding environment to its benefit and promote survival, and possibly by exposing the less abundant and metabolically active liver-stage parasite to NO-mediated killing. Interestingly, exogenous arginase activity in *L. major* or *H. pylori* infection similarly depletes host L-arginine levels and results in impaired T cell responses, and arginase inhibitors or supplemental L-arginine attenuates infection and parasite growth (*16*−*18*).

Analysis of *P. falciparum* arginase may explain decreased substrate and inhibitor potencies compared with that of human arginase I. Specifically, novel interactions are observed at the trimer interface due to the conserved 11-residue loop L8 insertion, and H381 of this loop extends from one monomer into the active site of an adjacent monomer in the trimer. The 74-residue LCR domain is disordered in the crystal structure, and its deletion does not affect substrate affinity. Thus, the three-dimensional structure of PFA promises to guide the future design and development of inhibitors that may be useful adjuvants in the treatment of malarial infections.

## ACKNOWLEDGMENT

This work is based upon research conducted at the Northeastern Collaborative Access Team beamlines of the Advanced Photon Source, which are supported by Grant RR-15301 from the National Center for Research Resources at the National Institutes of Health. Use of the Advanced Photon Source is supported by the U.S. Department of Energy, Office of Basic Energy Sciences, under Contract DE-AC02-06CH11357. We thank Dr. Scott Diamond for his assistance with kinetic colorimetric measurements and Dr. William DeGrado and Emma Magavern for assistance with the isothermal titration calorimetry measurements.

## REFERENCES

1. Snow, R. W., Guerra, C. A., Noor, A. M., Myint, H. Y., and Hay, S. I. (2005) The global distribution of clinical episodes of *Plasmodium falciparum* malaria. *Nature 434*, 214–217.
2. Greenwood, B. M., Fidock, D. A., Kyle, D. E., Kappe, S. H. I., Alonso, P. L., Collins, F. H., and Duffy, P. E. (2008) Malaria: Progress, perils, and prospects for eradication. *J. Clin. Invest. 118*, 1266–1276.
3. Centers for Disease Control and Prevention (2007) Malaria Surveillance: United States. Morbidity and Mortality Weekly Report, Vol. *58*, pp 1−10, Centers for Disease Control and Prevention, Atlanta.
4. World Health Organization (2009) World Malaria Report, pp 1−163, World Health Organization, Geneva.
5. Cox-Singh, J., Davis, T. M. E., Lee, K.-S., Shamsul, S. S. G., Matusop, A., Ratnam, S., Rahman, H. A., Conway, D. J., and Singh, B. (2008) *Plasmodium knowlesi* malaria in humans is widely distributed and potentially life threatening. *Clin. Infect. Dis. 46*, 165–171.
6. Winstanley, P. A., Ward, S. A., and Snow, R. W. (2002) Clinical status and implications of antimalarial drug resistance. *Microbes Infect. 4*, 157–164.
7. Kelly, J. X., Smilkstein, M. J., Brun, R., Wittlin, S., Cooper, R. A., Lane, K. D., Janowsky, A., Johnson, R. A., Dodean, R. A., Winter, R., Hinrichs, D. J., and Riscoe, M. K. (2009) Discovery of dual function acridones as a new antimalarial chemotype. *Nature 459*, 270–273.
8. Planche, T., Dzeing, A., Ngou-Milama, E., Kombila, M., and Stacpoole, P. W. (2005) Metabolic complications of severe malaria. *Curr. Top. Microbiol. Immunol. 295*, 105–136.
9. Mackintosh, C. L., Beeson, J. G., and Marsh, K. (2004) Clinical features and pathogenesis of severe malaria. *Trends Parasitol. 20*, 597–603.
10. Gramaglia, I., Sobolewski, P., Meays, D., Contreras, R., Nolan, J. P., Frangos, J. A., Intaglietta, M., and van der Heyde, H. C. (2006) Low nitric oxide bioavailability contributes to the genesis of experimental cerebral malaria. *Nat. Med. 12*, 1417–1422.
11. Yeo, T. W., Lampah, D. A., Gitawati, R., Tjitra, E., Kenangalem, E., McNeil, Y. R., Darcy, C. J., Granger, D. L., Weinberg, J. B., Lopansri, B. K., Price, R. N., Duffull, S. B., Celermajer, D. S., and Anstey, N. M. (2007) Impaired nitric oxide bioavailability and L-arginine-reversible endothelial dysfunction in adults with *falciparum* malaria. *J. Exp. Med. 204*, 2693–2704.
12. Olszewski, K. L., Morrisey, J. M., Wilinski, D., Burns, J. M., Vaidya, A. B., Rabinowitz, J. D., and Llinás, M. (2009) Host-parasite interactions revealed by *Plasmodium falciparum* metabolomics. *Cell Host Microbe 5*, 191–199.
13. Elford, B. C., Haynes, J. D., Chulay, J. D., and Wilson, R. J. M. (1985) Selective stage-specific changes in the permeability to small hydrophilic solutes of human erythrocytes infected with *Plasmodium falciparum*. *Mol. Biochem. Parasitol. 16*, 43–60.
14. Modolell, M., Corraliza, I. M., Link, F., Soler, G., and Eichmann, K. (1995) Reciprocal regulation of the nitric oxide synthase/arginase balance in mouse bone marrow-derived macrophages by TH1 and TH2 cytokines. *Eur. J. Immunol. 25*, 1101–1104.
15. Peranzoni, E., Marigo, I., Dolcetti, L., Ugel, S., Sonda, N., Taschin, E., Mantelli, B., Bronte, V., and Zanovello, P. (2007) Role of arginine metabolism in immunity and immunopathology. *Immunobiology 212*, 795–812.
16. Muleme, H. M., Reguera, R. M., Berard, A., Azinwi, R., Jia, P., Okwor, I. B., Beverley, S., and Uzonna, J. E. (2009) Infection with arginase-deficient *Leishmania major* reveals a parasite number-dependent and cytokine-independent regulation of host cellular arginase activity and disease pathogensis. *J. Immunol. 183*, 8068–8076.
17. Modolell, M., Choi, B.-S., Ryan, R. O., Hancock, M., Titus, R. G., Abebe, T., Hailu, A., Müller, I., Rogers, M. E., Bangham, C. R. M., Munder, M., and Kropf, P. (2009) Local suppression of T cell responses by arginase-induced L-arginine depletion in nonhealing leishmaniasis. *PLoS Negl. Trop. Dis. 3*, e480.
18. Chaturvedi, R., Asim, M., Lewis, N. D., Algood, H. M. S., Cover, T. L., Kim, P. Y., and Wilson, K. T. (2007) L-Arginine availability regulates inducible nitric oxide synthase-dependent host defense against *Helicobacter pylori*. *Infect. Immun. 75*, 4305–4315.
19. Weinberg, J. B., Lopansri, B. K., Mwaikambo, E., and Granger, D. L. (2008) Arginine, nitric oxide, carbon monoxide, and endothelial function in severe malaria. *Curr. Opin. Infect. Dis. 21*, 468–475.
20. Yeo, T. W., Lampah, D. A., Gitawati, R., Tjitra, E., Kenangalem, E., McNeil, Y. R., Darcy, C. J., Granger, D. L., Weinberg, J. B., Lopansri, B. K., Price, R. N., Duffull, S. B., Celermajer, D. S., and Anstey, N. M. (2008) Recovery of endothelial function in severe *falciparum* malaria: Relationship with improvement in plasma L-arginine and blood lactate concentrations. *J. Infect. Dis. 198*, 602–608.
21. Müller, I. B., Walter, R. D., and Wrenger, C. (2005) Structural metal dependency of the arginase from the human malaria parasite *Plasmodium falciparum*. *Biol. Chem. 386*, 117–126.
22. Wells, G. A., Müller, I. B., Wrenger, C., and Louw, A. I. (2009) The activity of *Plasmodium falciparum* arginase is mediated by a novel inter-monomer salt-bridge between Glu295-Arg404. *FEBS J. 276*, 3517–3530.
23. Aravind, L., Iyer, L. M., Wellems, T. E., and Miller, L. H. (2003) *Plasmodium* biology: Genomic gleanings. *Cell 115*, 771–785.
24. DePristo, M. A., Zilversmit, M. M., and Hartl, D. L. (2006) On the abundance, amino acid composition, and evolutionary dynamics of low-complexity regions in proteins. *Gene 378*, 19–30.

25. Gardner, M. J., Hall, N., Fung, E., White, O., Berriman, M., Hyman, R. W., Carlton, J. M., Pain, A., Nelson, K. E., Bowman, S., Paulsen, I. T., James, K., Eisen, J. A., Rutherford, K., Salzberg, S. L., Craig, A., Kyes, S., Chan, M.-S., Nene, V., Shallom, S. J., Suh, B., Peterson, J., Angiuoli, S., Pertea, M., Allen, J., Selengut, J., Haft, D., Mather, M. W., Vaidya, A. B., Martin, D. M. A., Fairlamb, A. H., Fraunholz, M. J., Roos, D. S., Ralph, S. A., McFadden, G. I., Cummings, L. M., Subramanian, G. M., Mungall, C., Venter, J. C., Carucci, D. J., Hoffman, S. L., Newbold, C., Davis, R. W., Fraser, C. M., and Barrell, B. (2002) Genome sequence of the human malaria parasite *Plasmodium falciparum*. *Nature 419*, 498–511.
26. Pizzi, E., and Frontali, C. (2001) Low-complexity regions in *Plasmodium falciparum* proteins. *Genome Res. 11*, 218–229.
27. Lavulo, L. T., Sossong, T. M., Jr., Brigham-Burke, M. R., Doyle, M. L., Cox, J. D., Christianson, D. W., and Ash, D. E. (2001) Subunit-subunit interactions in trimeric arginase. Generation of active monomers by mutation of a single amino acid. *J. Biol. Chem. 276*, 14242–14248.
28. Alarcón, R., Orellana, M. S., Neira, B., Uribe, E., García, J. R., and Carvajal, N. (2006) Mutational analysis of substrate recognition by human arginase type I: Agmatinase activity of the N130D variant. *FEBS J. 273*, 5625–5631.
29. Baggio, R., Elbaum, D., Kanyo, Z. F., Carroll, P. J., Cavalli, R. C., Ash, D. E., and Christianson, D. W. (1997) Inhibition of $Mn^{2+}{}_2$-arginase by borate leads to the design of a transition state analogue inhibitor, 2(*S*)-amino-6-boronohexanoic acid. *J. Am. Chem. Soc. 119*, 8107–8108.
30. Di Costanzo, L., Sabio, G., Mora, A., Rodriguez, P. C., Ochoa, A. C., Centeno, F., and Christianson, D. W. (2005) Crystal structure of human arginase I at 1.29-Å resolution and exploration of inhibition in the immune response. *Proc. Natl. Acad. Sci. U.S.A. 102*, 13058–13063.
31. Cama, E., Colleluori, D. M., Emig, F. A., Shin, H., Kim, S. W., Kim, N. N., Traish, A. M., Ash, D. E., and Christianson, D. W. (2003) Human arginase II: Crystal structure and physiological role in male and female sexual arousal. *Biochemistry 42*, 8445–8451.
32. Archibald, R. M. (1945) Colorimetric determination of urea. *J. Biol. Chem. 157*, 507–518.
33. Cheng, Y.-C., and Prusoff, W. H. (1973) Relationship between the inhibition constant ($K_I$) and the concentration of inhibitor which causes 50% inhibition ($I_{50}$) of an enzymatic reaction. *Biochem. Pharmacol. 22*, 3099–3108.
34. Otwinowski, Z., and Minor, W. (1997) Processing of X-ray diffraction data collected in oscillation mode. *Methods Enzymol. 276*, 307–326.
35. McCoy, A. J., Grosse-Kunstleve, R. W., Adams, P. D., Winn, M. D., Storoni, L. C., and Read, R. J. (2007) *Phaser* crystallographic software. *J. Appl. Crystallogr. 40*, 658–674.
36. Adams, P. D., Grosse-Kunstleve, R. W., Hung, L.-W., Ioerger, T. R., McCoy, A. J., Moriarty, N. W., Read, R. J., Sacchettini, J. C., Sauter, N. K., and Terwilliger, T. C. (2002) PHENIX: Building new software for automated crystallographic structure determination. *Acta Crystallogr. D58*, 1948–1954.
37. Emsley, P., and Cowtan, K. (2004) *Coot*: Model-building tools for molecular graphics. *Acta Crystallogr. D60*, 2126–2132.
38. Krissinel, E., and Henrick, K. (2007) Inference of macromolecular assemblies from crystalline state. *J. Mol. Biol. 372*, 774–797.
39. Bruña-Romero, O., Hafalla, J. C. R., González-Aseguinolaza, G., Sano, G., Tsuji, M., and Zavala, F. (2001) Detection of malaria liver-stages in mice infected through the bite of a single *Anopheles* mosquito using a highly sensitive real-time PCR. *Int. J. Parasitol. 31*, 1499–1502.
40. Cavalli, R. C., Burke, C. J., Soprano, D. R., Kawamoto, S., and Ash, D. E. (1994) Mutagenesis of rat liver arginase expressed in *Escherichia coli*: Role of conserved histidines. *Biochemistry 33*, 10652–10657.
41. García, D., Uribe, E., Lobos, M., Orellana, M. S., and Carvajal, N. (2009) Studies on the functional significance of a C-terminal S-shaped motif in human arginase type I: Essentiality for cooperative effects. *Arch. Biochem. Biophys. 481*, 16–20.
42. Colleluori, D. M., Morris, S. M., Jr., and Ash, D. E. (2001) Expression, purification, and characterization of human type II arginase. *Arch. Biochem. Biophys. 389*, 135–143.
43. Ryoo, S., Gupta, G., Benjo, A., Lim, H. K., Camara, A., Sikka, G., Lim, H. K., Sohi, J., Santhanam, L., Soucy, K., Tuday, E., Baraban, E., Ilies, M., Gerstenblith, G., Nyhan, D., Shoukas, A., Christianson, D. W., Alp, N. J., Champion, H. C., Huso, D., and Berkowitz, D. E. (2008) Endothelial arginase II: A novel target for the treatment of atherosclerosis. *Circ. Res. 102*, 923–932.
44. Birkholtz, L.-M., Wrenger, C., Joubert, F., Wells, G. A., Walter, R. D., and Louw, A. I. (2004) Parasite-specific inserts in the bifunctional S-adenosylmethionine decarboxylase/ornithine decarboxylase of *Plasmodium falciparum* modulate catalytic activities and domain interactions. *Biochem. J. 377*, 439–448.
45. Jean, L., Withers-Martinez, C., Hackett, F., and Blackman, M. J. (2005) Unique insertions within *Plasmodium falciparum* subtilisin-like protease-1 are crucial for enzyme maturation and activity. *Mol. Biochem. Parasitol. 144*, 187–197.
46. Yuvaniyama, J., Chitnumsub, P., Kamchonwongpaisan, S., Vanichtanankul, J., Sirawaraporn, W., Taylor, P., Walkinshaw, M. D., and Yuthavong, Y. (2003) Insights into antifolate resistance from malarial DHFR-TS structures. *Nat. Struct. Biol. 10*, 357–365.
47. Bewley, M. C., Jeffrey, P. D., Patchett, M. L., Kanyo, Z. F., and Baker, E. N. (1999) Crystal structures of *Bacillus caldovelox* arginase in complex with substrate and inhibitors reveal new insights into activation, inhibition and catalysis in the arginase superfamily. *Structure 7*, 435–448.
48. Kumarevel, T. S., Karthe, P., Kuramitsu, S., and Yokoyama, S. (2009) Crystal structure of the arginase from *Thermus thermophilus*. PDB entry 2EF4.
49. Cox, J. D., Kim, N. N., Traish, A. M., and Christianson, D. W. (1999) Arginase-boronic acid complex highlights a physiological role in erectile function. *Nat. Struct. Biol. 6*, 1043–1047.
50. Christianson, D. W. (2005) Arginase: Structure, mechanism, and physiological role in male and female sexual arousal. *Acc. Chem. Res. 38*, 191–201.
51. Ash, D. E., Scolnick, L. R., Kanyo, Z. F., Vockley, J. G., Cederbaum, S. D., and Christianson, D. W. (1998) Molecular basis of hyperargininemia: Structure-function consequences of mutations in human liver arginase. *Mol. Genet. Metab. 64*, 243–249.
52. Sabio, G., Mora, A., Rangel, M. A., Quesada, A., Marcos, C. F., Alonso, J. C., Soler, G., and Centeno, F. (2001) Glu-256 is a main structural determinant for oligomerisation of human arginase I. *FEBS Lett. 501*, 161–165.
53. Kanyo, Z. F., Scolnick, L. R., Ash, D. E., and Christianson, D. W. (1996) Structure of a unique binuclear manganese cluster in arginase. *Nature 383*, 554–557.
54. van Brummelen, A. C., Olszewski, K. L., Wilinski, D., Llinás, M., Louw, A. I., and Birkholtz, L. M. (2009) Co-inhibition of *Plasmodium falciparum* S-adenosylmethionine decarboxylase/ornithine decarboxylase reveals perturbation-specific compensatory mechanisms by transcriptome, proteome, and metabolome analyses. *J. Biol. Chem. 284*, 4635–4646.
55. Ochoa, A. C., Zea, A. H., Hernandez, C., and Rodriguez, P. C. (2007) Arginase, prostaglandins, and myeloid-derived suppressor cells in renal cell carcinoma. *Clin. Cancer Res. 13*, 721s–726s.
56. Zea, A. H., Rodriguez, P. C., Atkins, M. B., Hernandez, C., Signoretti, S., Zabaleta, J., McDermott, D., Quiceno, D., Youmans, A., O'Neill, A., Mier, J., and Ochoa, A. C. (2005) Arginase-producing myeloid suppressor cells in renal cell carcinoma patients: A mechanism of tumor evasion. *Cancer Res. 65*, 3044–3048.
57. Singh, R., Pervin, S., Karimi, A., Cederbaum, S., and Chaudhuri, G. (2000) Arginase activity in human breast cancer cell lines: N($\omega$)-Hydroxy-L-arginine selectively inhibits cell proliferation and induces apoptosis in MDA-MB-468 cells. *Cancer Res. 60*, 3305–3312.
58. Gobert, A. P., McGee, D. J., Akhtar, M., Mendz, G. L., Newton, J. C., Cheng, Y., Mobley, H. L. T., and Wilson, K. T. (2001) *Helicobacter pylori* arginase inhibits nitric oxide production by eukaryotic cells: A strategy for bacterial survival. *Proc. Natl. Acad. Sci. U.S.A. 98*, 13844–13849.
59. Cama, E., Pethe, S., Boucher, J. L., Han, S., Emig, F. A., Ash, D. E., Viola, R. E., Mansuy, D., and Christianson, D. W. (2004) Inhibitor coordination interactions in the binuclear manganese cluster of arginase. *Biochemistry 43*, 8987–8999.